Site selective spectroscopy and crystal field analysis of Er^{3+} in $Ca_3Ga_2Ge_3O_{12}$ garnet

2001 J. Phys.: Condens. Matter 13 8853

(http://iopscience.iop.org/0953-8984/13/39/311)

INSTITUTE OF PHYSICS PUBLISHING JOURNAL OF PHYSICS: CONDENSED MATTER

J. Phys.: Condens. Matter **13** (2001) 8853–8868 PII: S0953-8984(01)25142-X

Site selective spectroscopy and crystal field analysis of Er^{3+} in $Ca_3Ga_2Ge_3O_{12}$ garnet

R C Santana[1], J E Muñoz Santiuste[2], L A O Nunes[3], H C Basso[3] and M C Terrile[3]

[1] Instituto de Física, Universidade Federal de Goiás, Campus Samambaia, CP 131, 74001-970, Goiânia (GO), Brazil
[2] Departamento de Física, Escuela Politécnica Superior, Universidad Carlos III de Madrid, Avenida Universidad 30, Leganés E-28913, Madrid, Spain
[3] Departamento de Física e Informática, Instituto de Física de São Carlos, USP, Av. Dr Carlos Botelho, 1465, CP 369, 13560-970 São Carlos (SP), Brazil

Received 11 June 2001
Published 13 September 2001
Online at stacks.iop.org/JPhysCM/13/8853

Abstract

A detailed study of the optical spectroscopy of Er^{3+} in $Ca_3Ga_2Ge_3O_{12}$ crystals is reported. Several site selective techniques were employed (absorption, luminescence, excitation and up-conversion). The combined use of these techniques allowed the separation and classification of the observed spectral lines. Six different Er^{3+} optical centres are observed. The energy level analysis was performed using a parametric Hamiltonian for the $4f^{11}$ electronic configuration of Er^{3+} in a D_2 symmetry site. A set of parameters was obtained by fitting calculated to experimental energy levels for each identified centre. Differences among centres were analysed and related to the different charge compensating mechanisms.

1. Introduction

The role played by garnets in the development of solid state lasers is well known. Among them, $Ca_3Ga_2Ge_3O_{12}$ (CGGG) is interesting because of its low melting temperature (1400 °C). Stimulated emission has been reported in Nd^{3+}-doped CGGG crystals [1, 2]. More recently, Kaminskii *et al* [3] obtained stimulated Raman scattering in CGGG and proposed rare-earth doped CGGG as an active medium for a self-Raman shifted laser.

The interest in Er^{3+}-doped laser materials is related to the important applications of their intense infrared emissions. Particularly interesting is the emission at 2.8 μm ($^4I_{11/2} \rightarrow {}^4I_{13/2}$ transition). Laser emission in the region of water absorption (about 3 μm) is useful in medicine (surgery) and atmospheric humidity measurements [4]. Recently, theoretical results have been published about the kinetics of laser operation in the 3 μm region of several erbium-doped garnets [5]. In addition, common semiconductor lasers can excite this transition.

The CGGG garnet is disordered when doped with trivalent rare-earth ions. Er^{3+} ions incorporate into CGGG substituting Ca^{2+} ions in a dodecahedral D_2 site. As a consequence of the different valence between the active ion and the substituted crystal ion, charge compensation becomes necessary to maintain the electrical neutrality. Multicentres were detected in Nd^{3+}- and Er^{3+}-doped CGGG, by EPR [6] and optical spectroscopy [7–9]. They are associated with different compensating defects such as Ga^{3+} substituting Ge^{4+} in several non-equivalent positions (with different distances to the active ion) and the active ion in tetrahedral Ge^{4+} sites and Ca^{2+} sites, forming pairs [7, 8, 10].

The aim of the present work is to establish, as far as possible, the contribution of each individual centre to these spectra. Due to the superposition of lines originating in different centres, the analysis of the absorption and emission spectra is somewhat complicated. By combining several site selective spectroscopic techniques, emission, excitation and selective up-conversion, up to six sites were identified. The energy levels of the $^4I_{15/2}$ and $^4S_{3/2}$ states were univocally determined for all these centres.

Energy level positions were analysed using a semi-empirical Hamiltonian for the $4f^{11}$ configuration of Er^{3+} in D_2 symmetry sites. A set of free-ion and crystal field parameters, which properly reproduces the energy level scheme, was obtained for each individual site. The crystal field strength value, S, was obtained and compared with that for Er^{3+} ions in other garnets. Differences among centres were analysed and related to the different charge compensating mechanisms.

2. Experimental details

Single crystals of $Ca_3Ga_2Ge_3O_{12}$ were grown by the top seeded solution method, derived from the Czochralski and the flux excess methods [11]. The nominal erbium concentration was 0.5% in the melt. The samples were cut with faces perpendicular to the [001] direction and polished to optical quality. Low-temperature luminescence measurements were performed using a continuous-flow optical cryostat (Janis, ST-100), where the helium gas flow maintains a stable temperature of 4.6 K. A dye laser (Coumarin 540 for site selective luminescence measurements and DCM for excitation and selective up-conversion measurements) excited by a Coherent Innova 400 argon-ion laser provided the exciting energy. The emitted light was focused into the entrance slit of a 0.85 m Spex 1403 double monochromator and detected with an RCA-31034 photomultiplier connected to a PAR-128 lock-in amplifier. The resolution of the experimental set-up was less than 2 cm^{-1}.

Light absorption experiments at liquid helium temperature, 1.8 K, were performed in an immersion cryostat. The analysis was made using a 0.5 m Jarrel–Ash monochromator coupled to a Hamamatsu R636-10 photomultiplier, using a tungsten lamp as light source. For absorption measurements, the resolution was about 3 cm^{-1}.

3. Experimental results

The optical absorption spectra of Er^{3+}-doped crystals consist of a number of groups of lines corresponding to several transitions between the $^4I_{15/2}$ ground state and excited states inside the $4f^{11}$ configuration of the ion. Figure 1 shows the low-temperature (1.8 K) absorption spectrum of a Er^{3+}:CGGG sample in the visible and near-infrared regions. Transitions in this figure, covering $^4I_{13/2}$ to the $^2K_{15/2}$ final states, have been assigned by comparison with previously reported data [12, 13]. Energy positions of lines, listed in table 1, are labelled following the notation of Krupke and Gruber [14]. Energy positions of the $^4I_{15/2}$ Stark levels, obtained from

Table 1. Energy levels and centroid energy positions (cm^{-1}) for Er^{3+}-doped $Ca_3Ga_2Ge_3O_{12}$.

Multiplet (centroid)	Level[a]	Energy	Multiplet (centroid)	Level	Energy	Multiplet (centroid)	Multiplet Level	Energy	(centroid)	Multiplet Level	Energy	(centroid)	Multiplet Level	Energy	(centroid)	Level	Energy
$^4I_{15/2}$	Z_1	0	$^4I_{9/2}$	B_1	12 322	$^4S_{3/2}$	E_1	18 314	$^4F_{7/2}$	G_1	20 475		I_5	22 684		L_{14}	26 578
(248)[b]	Z_2	39	(12 512)	B_2	12 332	(18 375)	E_2	18 326	(20 601)	G_2	20 494					L_{15}	26 616
	Z_3	61		B_3	12 512		E_3	18 340		G_3	20 507	$^2H_{9/2}$	K_1	24 424			
	Z_4	94		B_4	12 524		E_4	18 349		G_4	20 520	(24 615)	K_2	24 441	$^2G_{9/2}$	M_1	27 315
	Z_5	330		B_5	12 530		E_5	18 361		G_5	20 555		K_3	24 457	(27 474)	M_2	27 339
	Z_6	391		B_6	12 541		E_6	18 376		G_6	20 570		K_4	24 578		M_3	27 363
	Z_7	507		B_7	12 564		E_7	18 404		G_7	20 584		K_5	24 596		M_4	27 387
	Z_8	559		B_8	12 583		E_8	18 415		G_8	20 647		K_6	24 625		M_5	27 462
				B_9	12 606		E_9	18 420		G_9	20 691		K_7	24 735		M_6	27 499
$^4I_{13/2}$	Y_1	6503					E_{10}	18 445		G_{10}	20 706		K_8	24 752		M_7	27 525
(6700)	Y_2	6561	$^4F_{9/2}$	D_1	15 246					G_{11}	20 716		K_9	24 781		M_8	27 555
	Y_3	6586	(15 372)	D_2	15 261	$^2H_{11/2}$	F_1	19 096		G_{12}	20 737		K_{10}	24 815		M_9	27 620
	Y_4	6603		D_3	15 277	(19 253)	F_2	19 113								M_{10}	27 673
	Y_5	6616		D_4	15 284		F_3	19 122	$^4F_{5/2}$	H_1	22 193	$^4G_{11/2}$	L_1	26 202			
	Y_6	6718		D_5	15 293		F_4	19 139	(22 255)	H_2	22 203	(26 417)	L_2	26 227	$^2K_{9/2}$	N_1	27 760
	Y_7	6739		D_6	15 313		F_5	19 158		H_3	22 221		L_3	26 266	(27 995)	N_2	27 835
	Y_8	6750		D_7	15 323		F_6	19 170		H_4	22 244		L_4	26 287		N_3	27 916
	Y_9	6777		D_8	15 340		F_7	19 179		H_5	22 257		L_5	26 328		N_4	28 037
	Y_{10}	6815		D_9	15 364		F_8	19 188		H_6	22 290		L_6	26 347		N_5	28 104
	Y_{11}	6845		D_{10}	15 398		F_9	19 326		H_7	22 305		L_7	26 361		N_6	28 135
	Y_{12}	6887		D_{11}	15 471		F_{10}	19 338		H_8	22 325		L_8	26 460		N_7	28 177
				D_{12}	15 479		F_{11}	19 347					L_9	26 520			
$^4I_{11/2}$	A_1	10 264		D_{13}	15 479		F_{12}	19 361	$^4F_{3/2}$	I_1	22 558		L_{10}	26 530			
(10 344)	A_2	10 354		D_{14}	15 506		F_{13}	19 371	(22 622)	I_2	22 583		L_{11}	26 538			
	A_3	10 415		D_{15}	15 520		F_{14}	19 387		I_3	22 614		L_{12}	26 550			
				D_{16}	15 547					I_4	22 671		L_{13}	26 564			

[a] Following the notation of Krupke and Gruber [14].
[b] From luminescence experiments under argon laser excitation (488 nm) [9].

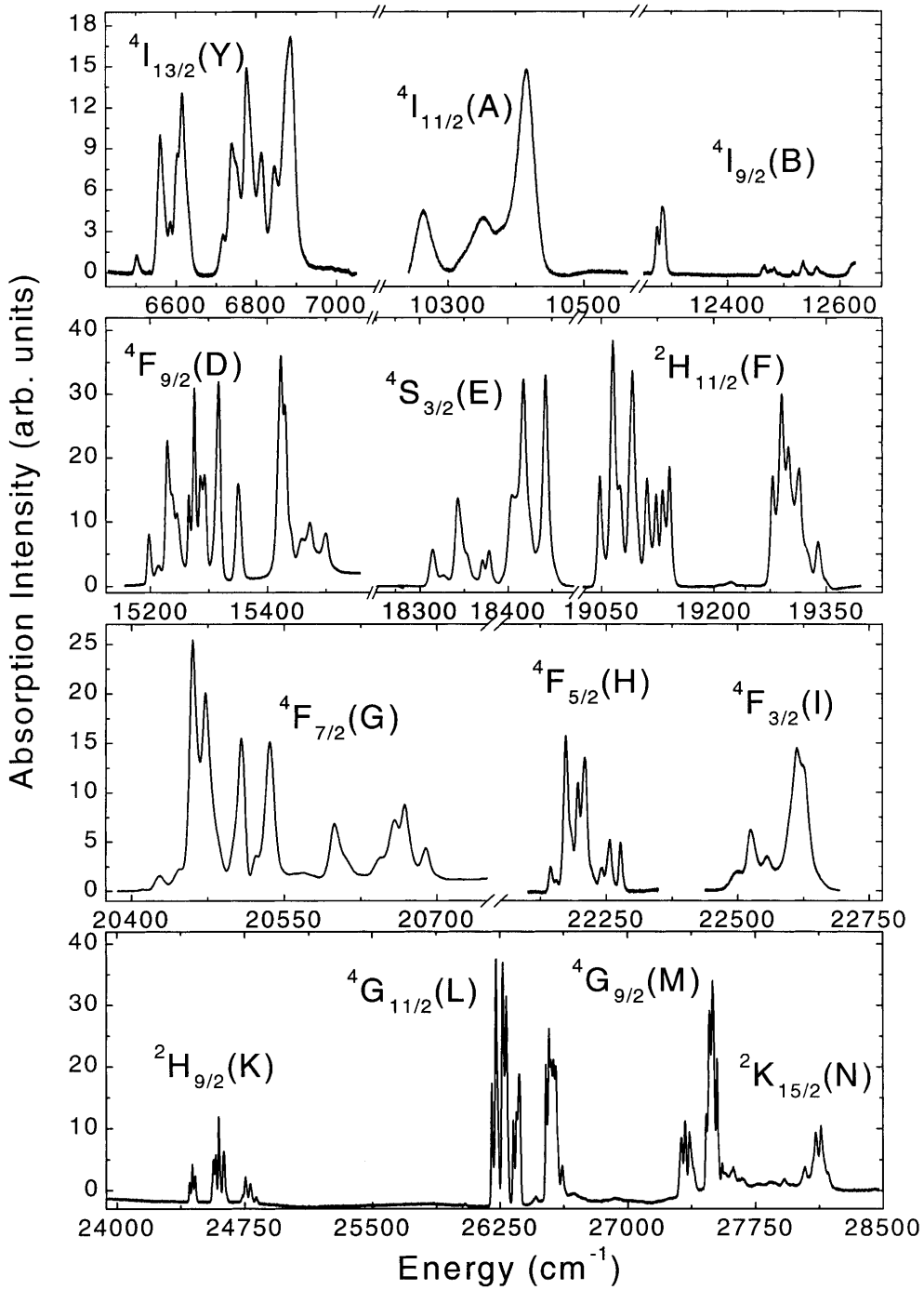

Figure 1. Absorption spectrum of Er^{3+} in $Ca_3Ga_2Ge_3O_{12}$ at 1.8 K. Final states involved in the transitions are indicated.

fluorescence measurements under Ar^+ laser excitation (488 nm), are also included in this table. All the absorption transitions show a surplus of lines. At this low temperature, only the lowest

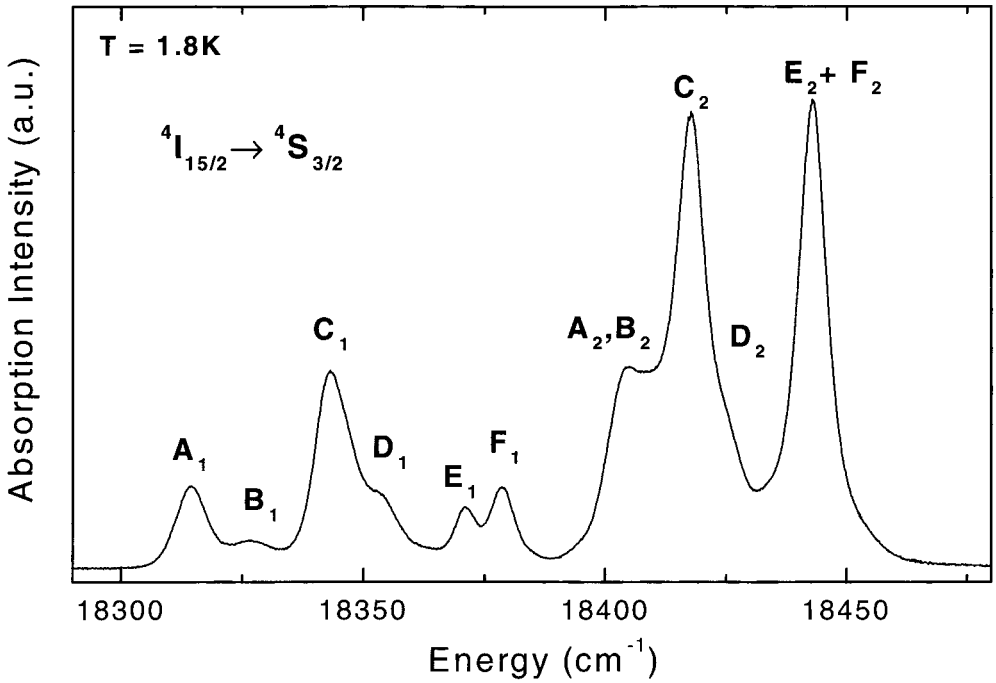

Figure 2. Absorption spectrum at 1.8 K corresponding to the $^4I_{15/2} \rightarrow {}^4S_{3/2}$ transition of the Er^{3+} ion in $Ca_3Ga_2Ge_3O_{12}$. See the text for an explanation of the labels.

Stark level of the $^4I_{15/2}$ state (a Kramers doublet hereafter labelled $^4I_{15/2}(0)$) is appreciably populated. Thus, the excess of lines must be attributed to the presence of multicentres in the crystal.

The low-temperature absorption spectrum displayed in figure 2 corresponds to the $^4I_{15/2}(0) \rightarrow {}^4S_{3/2}$ transition. The $^4S_{3/2}$ state is a quadruplet unfolded by the crystalline field into two Kramers doublets. Therefore, a maximum of two lines is expected in the absorption spectrum. However, nine lines are observed in the spectra indicating the presence of many different centres. Site selective measurements, discussed below, show that these lines originate in six different centres. Lines in figure 2 are labelled (in order of increasing energy) with letters A to F denoting different centres and with a subscript to indicate in which Kramers doublet (of the $^4S_{3/2}$ state) the transition originates.

Taking advantage of the well resolved structure of the $^4S_{3/2} \rightarrow {}^4I_{15/2}$ absorption transition, one of the simplest transitions in the absorption spectrum, site selective measurements were performed to obtain information about the level structure of each individual centre. Site selective emission measurements were performed adjusting the excitation energy to match the maximum of each absorption line in figure 2. In some cases, the overlap of the emission lines makes it difficult to distinguish the centre where the emission originates. Excitation spectra and selective up-conversion luminescence are useful as complements to resolve the energy level scheme.

Emission spectra obtained under selective excitation on the low-energy edge of the absorption spectrum, lines A_1 (18 314 cm^{-1}) and B_1 (18 326 cm^{-1}), are shown in figure 3. From these spectra six (centre A) and seven (centre B) of the expected lines for the $^4S_{3/2} \rightarrow {}^4I_{15/2}$ transition are observed. Obviously, the highest energy line, being coincident with the excitation energy, cannot be seen. Comparison with selective up-conversion luminescence results

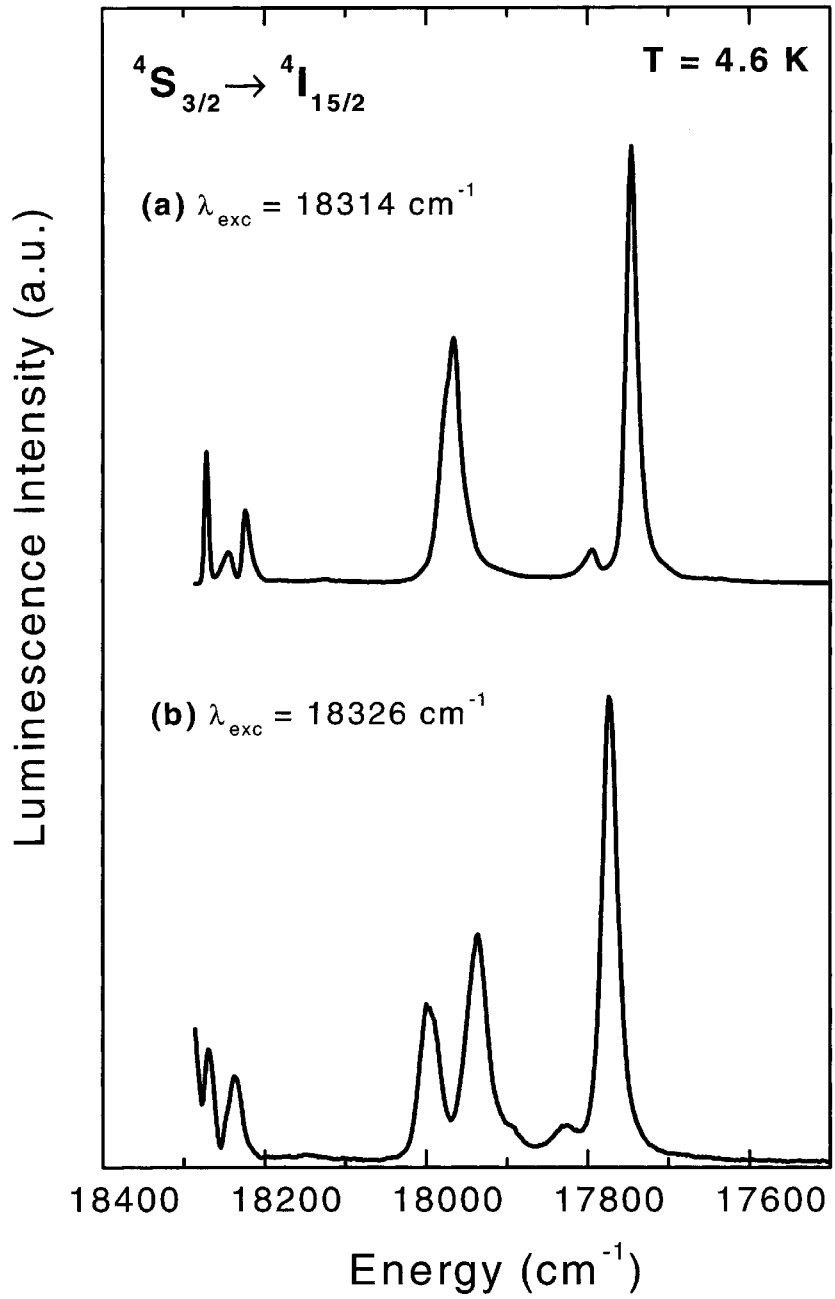

Figure 3. Low-temperature (4.6 K) site selective emission spectra for $^4S_{3/2} \rightarrow {}^4I_{15/2}$ for (a) centre A, $\lambda_{exc} = 18\,314$ cm^{-1} (line A_1 of the absorption spectrum in figure 2) and (b) centre B, $\lambda_{exc} = 18\,326$ cm^{-1} (line B_1).

permitted us to obtain the missing line in figure 3(a): the peak at 17 965 cm^{-1} is formed by two overlapping components. As an additional result, the emission under Ar^+ excitation (20 492 cm^{-1} coincident with the G_2 absorption line) corresponds to centre B.

Increasing difficulty to resolve centres was found when excitation lies in the region of the absorption spectrum corresponding to centres C and D, because of the superposition of lines and spectral diffusion. Exciting with energy centred at the peak labelled C_1 in the absorption spectra, the emission from sites A and B cannot be avoided. Patient work, comparing emissions under excitation in C_1 (18 340 cm^{-1}) and C_2 (18 415 cm^{-1}) peaks of the absorption spectrum (see figure 2), and up-conversion luminescence (exciting at 15 267 cm^{-1}), allowed us to obtain the energy level structure of the $^4I_{15/2}$ state attributed to the C centre. In this way it was also verified that the labelling of the absorption lines in figure 2 was correct. The assignation of lines attributed to centre D was obtained by eliminating those emission lines already identified as coming from the A, B and C centres.

Fortunately, luminescence spectra resulting from selective excitation in the absorption region corresponding to E and F centres also permit the separation of the lines corresponding to each centre. The emission spectra obtained under excitation at 18 368 (E_1), 18 376 (F_1) and 18 445 cm^{-1} ($E_2 + F_2$) are displayed together in figure 4 to evidence that the latter emission is a superposition of the first two.

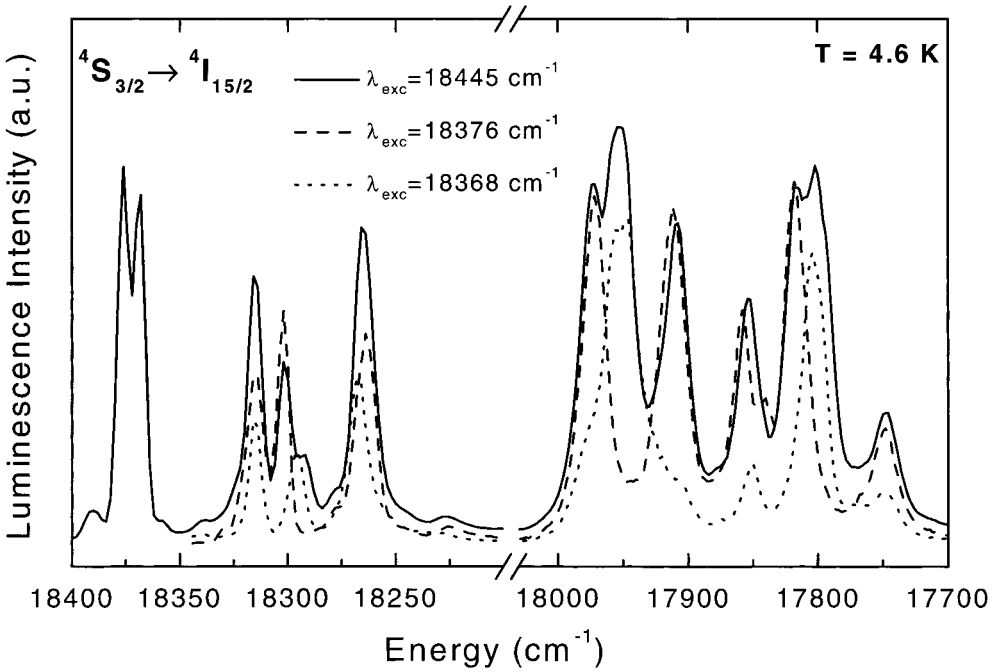

Figure 4. Low-temperature site selective emission spectra of the $^4S_{3/2} \rightarrow {}^4I_{15/2}$ transition. Dotted curve (centre E), $\lambda_{exc} = 18\,368\ cm^{-1}$ (line E_1 of the absorption spectrum in figure 2), dashed curve (centre F), $\lambda_{exc} = 18\,376\ cm^{-1}$ (line F_1), full curve (both E and F centres), $\lambda_{exc} = 18\,445\ cm^{-1}$ (lines E_1 and F_1).

The splitting of the $^4S_{3/2}$ excited state for most centres was obtained from excitation measurements. When the overlapping of emission lines from several centres made their assignation from excitation measurements difficult, the excited state splitting was determined from the analysis of the composition of the emission obtained under selective excitation in the higher energy absorption lines.

As an example, figure 5 shows the excitation spectra corresponding to emission from centres B and D. The spectrum in figure 5(a), obtained for the 17 746 cm^{-1} luminescence line

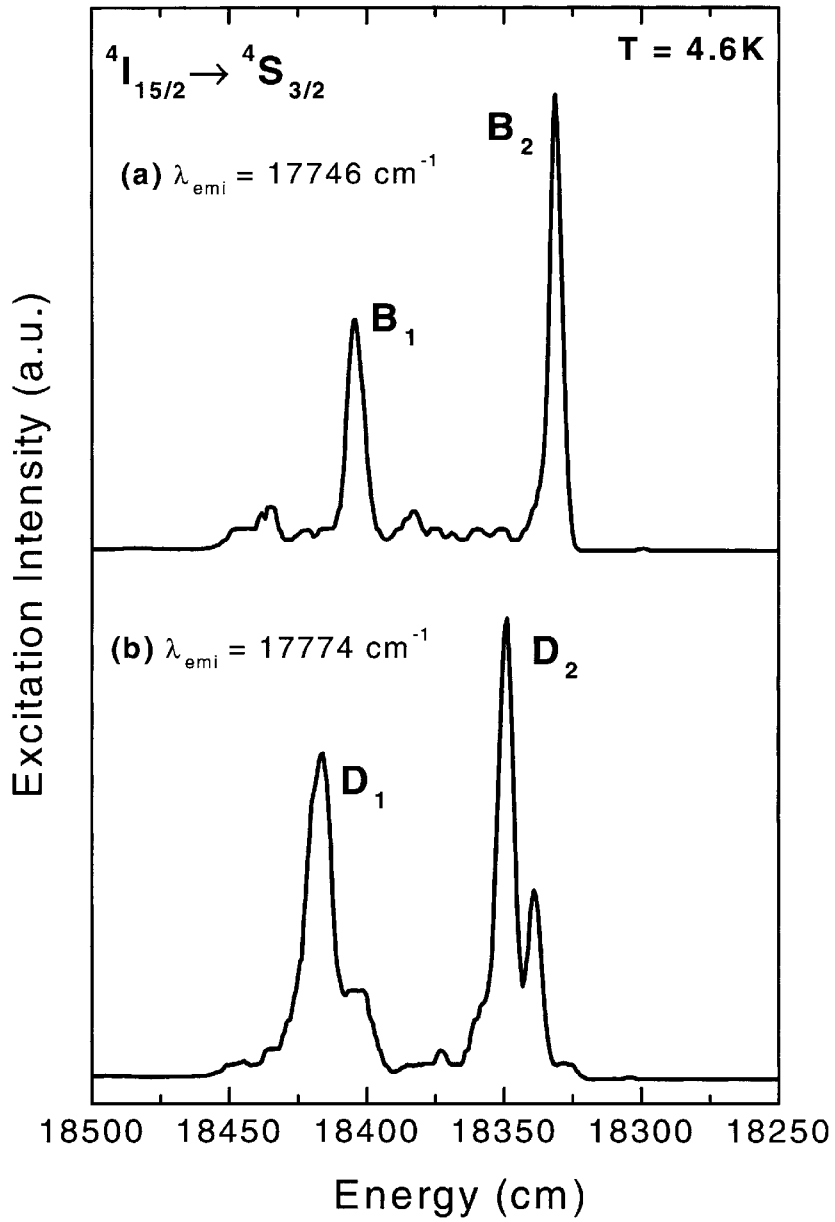

Figure 5. Low-temperature $^4I_{15/2} \rightarrow {}^4S_{3/2}$ excitation spectra: (a) centre A, monitoring the 17 746 cm^{-1} emission line, (b) centre D, monitoring the 17 774 cm^{-1} emission line.

(see figure 3), consists of just two lines located at 18 326 cm^{-1} (B_1) and 18 404 cm^{-1} (B_2) corresponding to the two $^4S_{3/2}$ stark levels of centre B. The excitation spectrum in figure 5(b) was obtained by detecting the luminescence at 17 774 cm^{-1}, the principal lines centred on 18 349 (D_1) and 18 420 cm^{-1} (D_2) constituting the pair of Kramers doublets related to site D.

Following this procedure all the Stark levels for the $^4I_{15/2}$ and $^4S_{3/2}$ states were obtained for each individual centre. Their energy level positions are listed in table 2.

Table 2. Calculated and experimental energy levels of the Er^{3+} ion in CGGG, for six identified sites. We list here only the energy levels of the $^4S_{3/2}$ and $^4I_{15/2}$ multiplets.

	Site A		Site B		Site C		Site D		Site E		Site F	
	Exp	Calc	Exp	Calc	Exp	Calc	Exp	Calc	Exp	Calc	Exp	Calc
$^4I_{15/2}$	0	−1	−4	−4	−13	−14	−27	−26	−44	−44	−54	−54
	38	14	35	29	20	15	25	18	8	−2	6	4
	64	79	57	58	33	39	53	45	28	28	20	21
	86	101	90	93	78	82	79	86	56	61	56	56
	331	314	326	325	372	363	336	336	376	373	250	251
	344	362	387	386	415	417	387	386	474	471	414	414
	516	523	503	505	485	492	523	524	490	492	468	468
	564	573	555	556	553	554	565	564	576	579	604	604
$^4S_{3/2}$	18 314	18 316	18 322	18 324	18 327	18 330	18 322	18 322	18 322	18 324	18 322	18 326
	18 404	18 401	18 400	18 402	18 402	18 399	18 393	18 392	18 401	18 399	18 391	18 386

3.1. Crystal field calculation

The usual Hamiltonian describing the energy level structure of the $4f^{11}$ electronic configuration for Er^{3+} in crystalline hosts includes the free-ion Hamiltonian and the crystal field perturbation. The free-ion Hamiltonian, accounting for the electrostatic repulsion, spin–orbit interaction and many-body corrections, is written as a sum, in the form

$$H_{FI} = \sum_n E^n e_n + \zeta A_{SO} + \alpha L(L+1) + \beta G(G_2) + \gamma G(R_7) + \sum_i T^i t_i + \sum_j P^j p_j + \sum_k M^k m_k$$

in which E^n ($n = 1, 2, 3$), ζ (the spin–orbit constant), α, β, γ, T^i ($i = 2, 3, 4, 6, 7, 8$), P^j ($j = 2, 4, 6$) and M^k ($k = 0, 2, 4$) are adjustable parameters (up to 20 free-ion parameters) and all other factors represent their associated angular operators [15, 16].

The crystal field Hamiltonian having the local D_2 symmetry of the Er^{3+} ion in the $Ca_3Ga_2Ge_3O_{12}$ garnet is given in Wybourne notation [17]:

$$H_{CF} = B_0^2 C_0^2 + B_2^2 (C_2^2 + C_{-2}^2) + B_0^4 C_0^4 + B_2^4 (C_2^4 + C_{-2}^4) + B_4^4 (C_4^4 + C_{-4}^4) + B_0^6 C_0^6 + B_2^6 (C_2^6 + C_{-2}^6) + B_4^6 (C_4^6 + C_{-4}^6) + B_6^6 (C_6^6 + C_{-6}^6)$$

with C_q^k being the renormalized spherical tensors from which matrix elements can be calculated and B_q^k the nine, all real, adjustable crystal field parameters.

The complete calculation of the $4f^{11}$ electronic configuration of Er^{3+} involves the diagonalization of a 364×364 $LSJM_J$ matrix using a Hamiltonian with 29 parameters (20 free-ion parameters and nine crystal field parameters for D_2 local symmetry), to obtain the position of 182 energy levels (Kramers doublets). The experimental data set presented in table 1 includes 139 Stark levels spanning 14 LSJ states. These energy levels are related to six optical centres. Under these conditions we can obtain a set of parameters for each particular centre taking advantage of the well resolved $^4I_{15/2}$ and $^4S_{3/2}$ states. For these states, the energy level positions (reported in table 2) have been univocally related to each individual centre. The approximation to the energy levels was made in two steps.

First, the 14 experimental centroid energies of the LSJ multiplets (an averaged value for all centres) were fitted using the free-ion Hamiltonian in an iterative procedure: starting from electrostatic and spin–orbit interaction and gradually including many-body and magnetic interactions. The free-ion parameters given by Carnall *et al* [18] were used as initial values. The large number of free-ion parameters was reduced in the usual way by fixing all T^{i}, P^j

and M^k parameters to adequate values obtained by extensive computational work. Thus, only eight of the free-ion parameters were treated as independent fitting variables in the final fitting procedure. This reduced set of parameters accurately reproduces the 14 LSJ centroid energies without serious degradation of the quality of the fit.

The second step involves the crystal field Hamiltonian and the experimental Stark levels. The actual total Hamiltonian has 17 parameters (nine crystal field parameters for D_2 local symmetry are added to the eight parameters of the restricted free-ion Hamiltonian). The well resolved Stark level positions of the $^4I_{15/2}$ and $^4S_{3/2}$ states for each particular centre were used. Additional energy levels were selected from the more intense absorption lines from other multiplets. Those levels which are mainly related to the fitted centre, as discussed for the G_2 level in table 1 related to centre B, were used. At least 25 experimental energy levels were used in this calculation to fit 17 parameters. A weighted function was used to force the fitting to the well determined $^4I_{15/2}$ and $^4S_{3/2}$ Stark levels.

Calculations were performed on a personal computer using a suitable set of parameters to start with and the parameters were refined by means of the least-squares method. Initial values of crystal field parameters were obtained by means of the single overlap model [19] over the D_2 sites on the garnet using x-ray data of a $Ca_3Ga_2Ge_3O_{12}$ crystal [20].

The final parameters for each site are presented in table 3. The energy levels for each particular centre calculated using these parameters are included in table 2. A graphical illustration of the experimental (right) and calculated (left) level scheme is given in figure 6 for the well resolved $^4I_{15/2}$ and $^4S_{3/2}$ states. The fitting gives accurate results except for the centre A.

Table 3. Hamiltonian parameters in cm^{-1} and crystal field strength values obtained from the fit of levels of the different erbium centres in the CGGG:Er^{3+} crystal.

Parameter[a]	Site A	Site B	Site C	Site D	Site E	Site F
E^1	6658	6666	6668	6664	6667	6661
E^2	32.6	32.5	32.5	32.6	32.5	32.5
E^3	669	669	668	668	669	669
ζ	2343	2345	2345	2344	2343	2349
α	26.6	26.5	26.5	26.4	26.5	26.5
β	−800	−814	−813	−800	−802	−804
γ	1776	1780	1780	1777	1775	1777
B_0^2	1261	1146	1001	1166	1141	1014
B_2^2	−756	−658	−416	−679	−239	−1015
B_0^4	453	838	661	1080	890	790
B_2^4	−481	−255	−30	−467	−128	309
B_4^4	1677	1564	1675	1379	1818	1568
B_0^6	−525	−633	−612	−817	−696	−385
B_2^6	−57	−96	−43	−147	−124	26
B_4^6	576	600	798	626	859	758
B_6^6	−71	−65	8	52	−82	−306
S	663	622	597	625	649	675

[a] The following parameters were held fixed in the data fits: $T^2 = 457$, $T^3 = 54$, $T^4 = 92$, $T^6 = -572$, $T^7 = 163$, $T^8 = 222$, $M^0 = 2.6$, $P^2 = 431$. The usual relationships, $M^2 = 0.56\,M^0$, $M^4 = 0.38\,M^0$, $P^4 = 0.75\,P^2$, $P^6 = 0.75\,P^2$, were also used.

As expected, only small changes among the optical centres are observed for the free-ion parameters (see table 3), and their values are similar to those published for other Er^{3+}-doped crystals [13]. The obtained crystal field parameters are characterized by large values of B_0^2

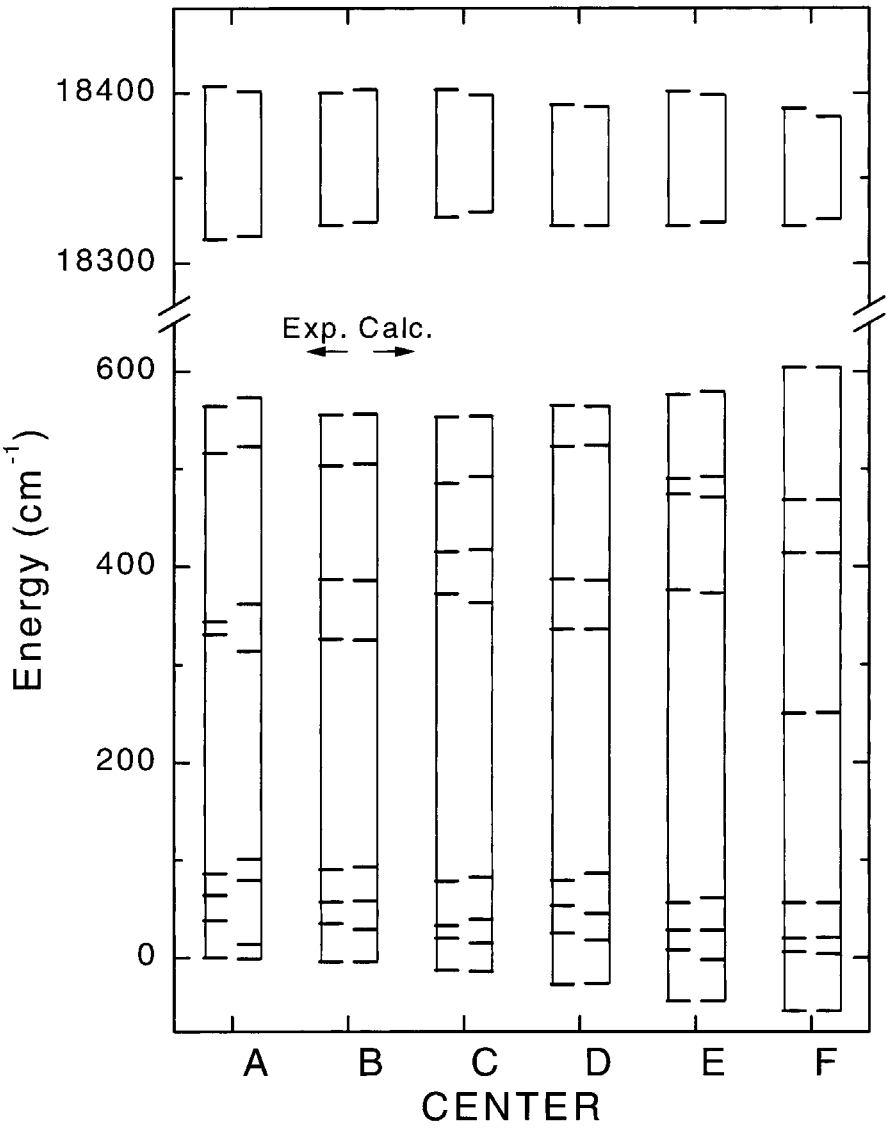

Figure 6. Schematic diagram showing the experimental and calculated energy levels in CGGG:Er^{3+} for the well resolved $^4I_{15/2}$ and $^4S_{3/2}$ states.

and B_4^4, small values of B_2^6 and B_6^6 and intermediate values for the rest of the parameters. We also note the strong variations among centres of some parameters.

For D_2 sites in garnets, six equivalent sets of crystal field parameters can be defined from rotations. This fact makes the comparison with published results for Er^{3+} ions in other garnets very difficult. Moreover, in CGGG the $Er^{3+}(Ca^{2+})$ substitution requires the presence of a charge compensation mechanism in the neighbourhood of the Er^{3+} ion. Different charge compensation mechanisms may perturb the local environment of Er^{3+} ions from non-equivalent directions. As we have already stated, centre-to-centre differences in this crystal must be related to the several charge compensation possibilities [7, 8, 10] that account for different potentials over

non-equivalent sites occupied by erbium ions. Thus, several choices of principal axis must be taken into account to compare the obtained CF parameters among centres or with previous results. To avoid the problem of axis selection, the values of the rotationally invariant crystal field strength, defined as

$$S = \sqrt{\frac{1}{3}\sum_{k=2,4,6}\frac{1}{2k+1}\left[(B_0^k)^2 + 2\sum_{q>0}(B_q^k)^2\right]}$$

are also included in table 3 for each centre. The obtained S value varies among centres from 597 to 675 cm^{-1}. For comparison purposes table 4 shows the relevant parameters of Er^{3+} in other garnets. The mean S value, 638 cm^{-1}, obtained for Er^{3+} in CGGG is similar to those obtained in yttrium garnets.

Table 4. Lattice parameters (a_0), Er–O distances and crystal field strength parameter, S, for YAG:Er, YSAG:Er and CGGG:Er crystals.

	Er–O distances (Å)			
Host	R_1	R_2	a_0 (Å)	S (cm^{-1})
YAG:Er	2.303[a]	2.432[a]	12.000[a]	626[c]
YSAG:Er	2.338[b]	2.440[b]	12.271[b]	637[c]
CGGG:Er	2.380[a]	2.506[a]	12.250[a]	638[d]

[a] [20].
[b] [25].
[c] The S parameter for $Y_3Al_5O_{12}:Er^{3+}$ (YAG:Er) and $Y_3Sc_2Al_3O_{12}:Er^{3+}$ (YSAG:Er) was calculated from no CCF parameters obtained by Gruber *et al* [13].
[d] The S value for CGGG is the averaged value for all centres in table 3.

Previous studies in Nd^{3+}-doped YAG [21] showed that, for any axis set selection, the B_2^k and B_6^k parameters are always lower than B_0^k and B_4^k, and an approximated D_{2d} symmetry (in which B_2^k and B_6^k are ruled out) can be successfully used to reproduce the level scheme. At this point it is interesting to note that in yttrium garnets rare-earth ions replace Y^{3+} ions and no charge compensation is needed.

From our result, B_2^6 and B_6^6 are very low for all centres but B_2^4 and B_2^2 are relatively low only for centres labelled C and E. The rank six crystal field parameters represent the short distance interaction, being very sensitive to changes in the electrostatic interaction between the lanthanum ion and the ligand oxygen ions in the first coordination sphere. Their relatively small variations among centres indicate that the short-range environment is similar for all centres. Moreover, the low contribution of rank six parameters to the total S value ($\sim$5% of the total value) indicates that the variation in the S value among centres is mainly related to changes in the parameters of ranks two and four accounting for medium and long distance effects. This fact is in agreement with the hypothesis of similar short-range environments for all centres, the most important difference among centres being the location of the charge compensating defect in the vicinity of the erbium ion, outside the first coordination sphere. The large B_0^2 values obtained, associated with the strong observed $^4S_{3/2}$ splitting, are related to the strong axial distortion over the $Er^{3+}(Ca^{2+})$ ion-charge compensation defect axis.

The low values of B_2^4 and B_2^2 obtained for centres C and E indicate that the charge compensating defect is located far away from the $Er^{3+}(Ca^{2+})$ ion, maintaining the approximated D_{2d} symmetry. The lower the distance between the $Er^{3+}(Ca^{2+})$ ion and the charge compensation defect, the stronger the distortion is. This fact results in an increase of the values of B_2^4 and B_2^2 parameters, as observed for most of the centres, and the approximated D_{2d} symmetry is no longer valid.

The maximum splitting, due to the crystal field, of a J-manifold is in some way directly proportional to the total crystal field strength [22], but with the general restriction that only the B_k^q involved in the degeneracy removal of the J-manifold must be included in the crystal field strength [23, 24]. Figure 7 displays the total splitting of the $^4I_{15/2}$ and $^4S_{3/2}$ multiplets and the resulting S values for each centre. A linear behaviour is observed between the S values and the $^4I_{15/2}$ total splitting among centres F to C (and probably B). Centre A appears to be out of this linear relation. This different behaviour, the low accuracy of the obtained fitting and the high $^4S_{3/2}$ splitting obtained for centre A appear to indicate a different origin. The $^4S_{3/2}$ total splitting (not shown in the figure) does not follow a clear relation with the S value among centres, even if only B_q^2 parameters are used. This fact may obviously be due to the limitations of the fitting procedure.

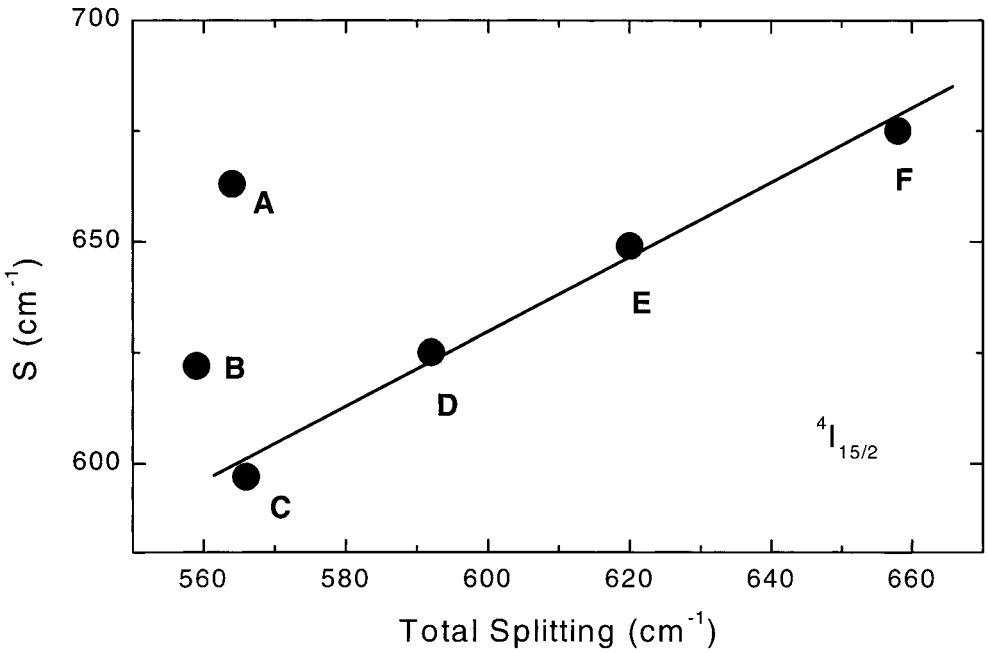

Figure 7. Total splitting of the $^4I_{15/2}$ state versus crystal field strength for each centre of the Er^{3+} in the CGGG system. The full line is only to guide the eye.

Let us try to comment briefly on the several non-equivalent charge compensation configurations proposed. Because both ions have a similar radius, the substitution (Ga^{3+}(Ge^{4+})) appears as a feasible candidate for the charge compensation mechanism. Figure 8 displays an octant of the CGGG structure showing all cationic sites and the local oxygen environment of a Ca^{2+} ion. Four possibilities for non-equivalent positions (different distances to the active ion) of compensating defects such as Ga^{3+} substituting Ge^{4+} are indicated by arrows and the distances to the active ion (Er^{3+}(Ca^{2+})) are shown. A similar behaviour is expected for those Er^{3+} ions in Ca^{2+} sites having Ga^{3+}(Ge^{4+}) as compensating defects, for which the crystal field intensity depends on the distance between Er^{3+}(Ca^{2+}) and the charge compensation defect. The obtained linear relation between the crystal field strength and total splitting among centres C to F points to a relation of these centres to the Er^{3+}(Ca^{2+}) ions having Ga^{3+}(Ge^{4+}) as compensating defects. We speculate on the possible relation of charge compensating (Ga^{3+}(Ge^{4+})) defects at long distances (about 6 Å) for C and E centres. As already mentioned, the low values

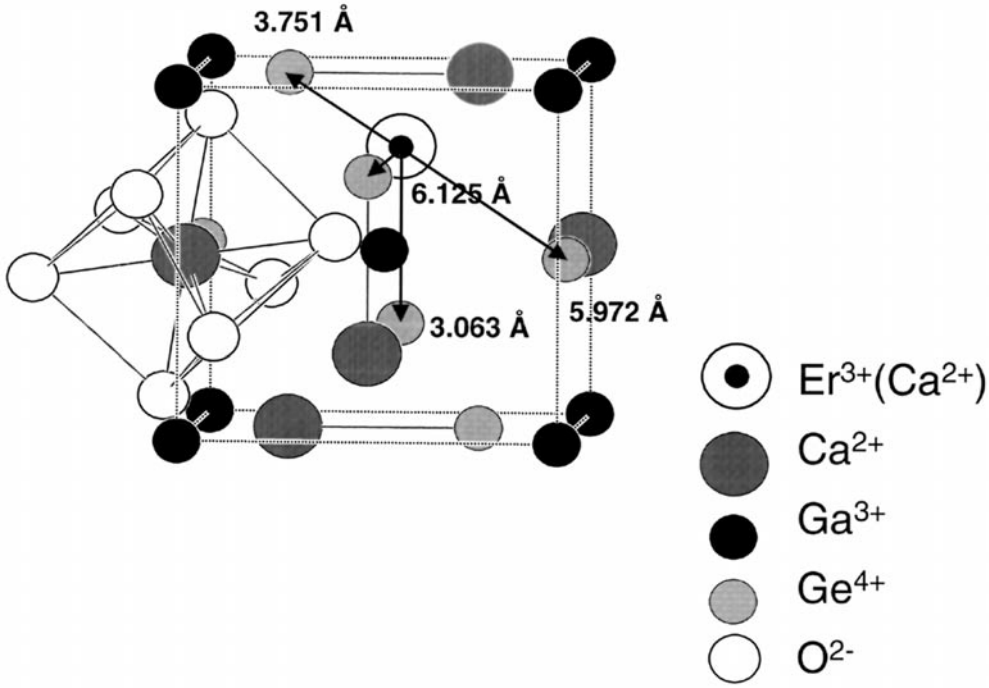

Figure 8. Cationic locations of the CGGG lattice. The four nearest Ge^{4+} neighbours of the Er^{3+} (Ca^{2+}) site are indicated by arrows and their distances reported. The oxygen environment of a Ca^{2+} ion is also depicted.

of B_2^k and B_6^k parameters obtained for centres C and E are indicative of an approximated D_{2d} symmetry, and suggest a long-range compensation mechanism (low distorted centres). Centre C has the highest absorption bands. Assuming similar absorption cross sections for all centres, the absorption intensity must be associated with the number of ions occupying this centre. This fact could indicate a preference for a distant location of (Ga^{3+}(Ge^{4+})) acting as a charge compensation mechanism. Only two and four equivalent lattice positions are available for the nearest and second neighbour (Ga^{3+}(Ge^{4+})) sites while eight and four possibilities are available for sites located far away. This could be the origin of this preference.

Pairs (Er^{3+}(Ca^{2+}))–(Er^{3+}(Ge^{4+})) were also proposed as charge compensating defects. The sample considered in this work was too diluted (0.5% Er), but the possibility of pairs cannot be disregarded. The (Er^{3+}(Ge^{4+}) substitution means a strong distortion of the crystal lattice because of the difference in ionic radii (R(Er) = 1.04 Å, R(Ge) = 0.55 Å). Thus a strong crystal field is expected for this centre. The high $^4I_{15/2}$ splitting obtained for centre A could be indicative of the possibility of (Er^{3+}(Ge^{4+})) substitution. The different behaviour obtained for centre A, as already discussed, supports this hypothesis. In any case, other possibilities of charge compensation mechanisms can also be taken into account. Additional experimental results by different techniques are needed to give a definitive explanation of the centres.

4. Conclusions

In this paper we report energy level data and analysis of the $4f^{11}$ electronic configuration of Er^{3+} in $Ca_3Ga_2Ge_3O_{12}$ garnet. In spite of the spectral complexity, we could separate the contribution of six different sites.

From the analysis of optical measurements, visible and infrared, the energy levels of Er^{3+} in CGGG crystals were evaluated. As it was evident that the optical spectra were a superposition of absorption (or emissions) arising from different Er^{3+} centres, site selective emission, excitation and up-conversion spectroscopic techniques were applied. In this way six sets of lines were separated for $^4S_{3/2}$ and $^4I_{15/2}$ states. The usual semi-empirical Hamiltonian was used in the analysis of the six sets of energy levels: those separated for $^4S_{3/2}$ and $^4I_{15/2}$ states completed with a choice of levels of other states.

An appropriate weighed function was necessary to force the fitting of the separated states. A good agreement was obtained for all the centres, except one (centre A) assuming D_2 symmetry. The free-ion parameters are almost identical among centres and similar to those reported for erbium in other crystals.

Six different crystal field parameter sets are obtained, with crystal field strength similar to those found in other erbium-doped garnets. Differences among centres are interpreted as due to the presence of several possible charge compensation mechanisms induced by Er^{3+} (Ca^{2+}) substitution. This fact induces an axial distortion over the D_2 symmetry, the intensity of which depends on the distance between Er^{3+}(Ca^{2+}) and the charge compensation defect. A similar behaviour is expected for those Er^{3+} ions in Ca^{2+} sites having Ga^{3+}(Ge^{4+}) as nearest, next-nearest and farther compensating defects, as seen for centres labelled C to F. Erbium ions located in Ge^{4+} sites, forming pairs with other Er^{3+}(Ca^{2+}) ions could explain the centre A. Of course as this is a highly nonlinear fitting, it is necessary to be careful in the interpretation of the results.

Acknowledgments

We are grateful to H P Jensen, who kindly provided us with samples. This work was supported by FAPESP, São Paulo, SP, Brazil, CNPq, Brazil, CAPES, Brazil and FINEP, Brazil.

References

[1] Kaminskii A A, Mill B V and Butashin A V 1983 *Phys. Status Solidi* a **78** 723
[2] Jaque D, Caldiño G U and García Solé J 1999 *J. Appl. Phys.* **86** 6627
[3] Kaminskii A A, Eichler H J, Fernandez J, Findeisen J, Balda R and Buytashin A V 1988 *Phys. Status Solidi* b **207** R3
[4] Stoneman R C and Esterowitz L 1990 *Opt. Photon.* **8** 10
[5] Tikerpae M, Jackson S D and King T A 1988 *J. Mod. Opt.* **45** 1269
[6] Moraes I J, de Souza R R, Nascimento O R, Terrile M C and Barberis G E 1995 *Solid State Commun.* **95** 251
[7] Caldiño G U, Voda M, Jaque F, García Solé J and Kaminskii A A 1993 *Chem. Phys. Lett.* **213** 84
[8] Caldiño G U, Bausá L E, García Solé J, Jaque F, Kaminskii A A, Butashin A V and Mill B V 1994 *J. Physique Coll.* IV C4 389
[9] Santana R C, Nunes L A O, Basso H C, Terrile M C and Barberis G E 1998 *Solid State Commun.* **106** 463
[10] Eskov N A, Osiko V V, Sobol A A, Timosheehkin M I, Butaeva T I, Chan Ngok and Kaminskii A A 1987 *Izv. Akad. Nauk. SSR Ser. Neog. Mater.* **14** 2254
[11] Simonaitis V K 1986 *Characterization of Cr,Er:$Ca_3Ga_2Ge_3O_{12}$ of a Laser Crystal* (MIT)
[12] Dieke G H 1968 *Spectra and Energy Levels of Rare Earth Ions in Crystals* (New York: Wiley-Interscience)
[13] Gruber J B, Quagliano J R, Reid M F, Richardson F S, Hills M E, Seltzer M D, Stevens S B, Morrison C A and Allik T H 1993 *Phys. Rev.* B **48** 15 561
[14] Krupke W F and Gruber J B 1963 *J. Chem. Phys.* **39** 1024
[15] Carnall W T, Goodman G L, Rajnak K and Rana R S 1989 *J. Chem. Phys.* **90** 3443
[16] Morrison C A 1988 *Angular Momentum Theory Applied to Interaction in Solids* (Berlin: Springer)
[17] Wybourne B G 1965 *Spectroscopy Properties of Rare Earths* (New York: Wiley)
[18] Carnall W T, Fields P R and Rajnak K 1968 *J. Chem. Phys.* **49** 4424
[19] Malta O L 1982 *Chem. Phys. Lett.* **87** 27

Malta O L 1982 *Chem. Phys. Lett.* **88** 353
[20] Novak P and Vosika L 1983 *Czech. J. Phys.* B **33** 1135
[21] Morrison C A, Wortman D E and Karayanis N 1976 *Rare Earth Ion–Host Lattice Interactions Lanthanides in* $Y_3Al_5O_{12}$ (Fort Monmounth, NJ: Harry Diamond Laboratories)
[22] Auzel F 1979 *Mater. Res. Bull.* **14** 223
[23] Auzel F and Malta O L 1983 *J. Physique* **44** 201
[24] Malta O L, Antic-Fidancev E, Lemaitre-Blaise M, Milicic-Tang A and Taibi M 1995 *J. Alloys Compounds* **228** 41
[25] Allik T H, Morrison C A, Gruber J B and Kokta M R 1990 *Phys. Rev.* B **41** 21